2018

Fluid Flow through Front Clearances of Dry Running Screw Machines Using Dimensionless Numbers

Matthias Utri
Chair of Fluidics, TU Dortmund University, Germany, matthias.utri@tu-dortmund.de

Andreas Bruemmer
TU Dortmund University, Germany, andreas.bruemmer@tu-dortmund.de

Fluid Flow through Front Clearances of Dry Running Screw Machines Using Dimensionless Numbers

Matthias Utri[1]*, Andreas Brümmer[2]

[1]TU Dortmund University, Chair of Fluidics,
Dortmund, Germany
Phone: +49 231 755 5724, Fax: +49 231 755 5722
E-mail: matthias.utri@tu-dortmund.de

[2]TU Dortmund University, Chair of Fluidics,
Dortmund, Germany
Phone: +49 231 755 5720, Fax: +49 231 755 5722
E-mail: andreas.bruemmer@tu-dortmund.de

* Corresponding Author

ABSTRACT

Chamber model simulation is a common approach for the simulation of positive displacement machines. For this kind of simulation, clearance mass flow is usually predicted using an isentropic estimation, which is corrected with a flow coefficient in order to account for the real flow conditions and the corresponding mass flow. Detailed knowledge of the flow coefficient and its dependencies is crucial for a meaningful simulation of positive displacement machines. This paper investigates the two-dimensional fluid flow through the front clearance (also called end clearance) of twin screw compressors where leakage paths have one stationary and one moving boundary. Dimensionless numbers are determined using the Pi-theorem and are varied systematically in order to show their individual influence on front clearance mass flow rate. The results are therefore useful for any dry running application with similar clearance geometry, independent of the type of gas (e.g. heat capacity, viscosity) and operating conditions (e.g. pressure, temperature, rotational speed). Mass flow is determined using CFD simulation and compared to analytical solutions and experimental data.

1. INTRODUCTION

Screw machines used for the compression of gaseous fluids can be found in numerous engineering applications. Two different simulation principles are suitable for the prediction of the operational behavior of screw machines, CFD simulation (e.g. Rane et. al., 2014) and chamber model simulation (e.g. Kauder et. al, 2002). CFD simulation is often used for detailed simulation of individual machines or machine parts. However, due to the challenges in meshing of the working chambers and the time-consuming computation, chamber model simulation is a more efficient approach and often suitable when many configurations need to be simulated, e.g. for the optimization of geometric parameters. Chamber model simulation is based on a zero-dimensional chamber model which includes all time-dependent geometrical values of chamber volumes, clearance and port areas. The fluid states inside all working chambers are calculated simultaneously, where the fluid is assumed to be homogeneous and motionless. Port and clearance areas allow exchange of mass and energy between the chambers. These exchanges can usually be estimated with simple representations such as an isentropic nozzle flow - this pure pressure induced mass flow rate can be estimated as shown in eq. (1) (Saint Venant and Wantzel, 1839):

$$\dot{m}_{th} = \rho_c \cdot A_c \cdot c_c = p_{hp} \cdot A_c \cdot \sqrt{\frac{2 \cdot \kappa}{(\kappa - 1) \cdot R_s \cdot T_{hp}} \cdot \left((\Pi_c)^{\frac{2}{\kappa}} - (\Pi_c)^{\frac{\kappa+1}{\kappa}} \right)}, \quad \frac{p_{lp}}{p_{hp}} = \Pi_c > \Pi_{crit} \tag{1}$$

Eq. (1) assumes adiabatic, frictionless flow from a volume with higher pressure (index hp) through an area A_c to a volume with lower pressure (index lp). If the cross section of the flow channel varies in flow direction, A_c is the

minimum area. The equation assumes the low pressure to be present in this minimum flow cross section and is valid for subcritical pressure ratios $\Pi_c > \Pi_{crit}$. When the pressure ratio $\Pi_c \in [0, 1]$ is below the critical pressure ratio Π_{crit}, mass flow rate is independent from the low pressure conditions and can be calculated by eq. (2), representing the sonic velocity in the minimum flow cross section.

$$\dot{m}_{th} = \rho_c \cdot A_c \cdot a_c = \rho_c \cdot A_c \cdot \sqrt{\kappa \cdot R_s \cdot T_c} = p_{hp} \cdot A_c \cdot \sqrt{\frac{2\kappa}{(\kappa+1) \cdot R_s \cdot T_{hp}}} \cdot \left(\frac{2}{\kappa+1}\right)^{\frac{1}{\kappa-1}}, \quad \Pi_c < \Pi_{crit} \tag{2}$$

To take friction and contraction of the flow into account, the theoretical mass flow is usually adjusted using a flow coefficient α:

$$\dot{m}_{real} = \alpha \cdot \dot{m}_{th} \tag{3}$$

This flow coefficient is a crucial parameter for a meaningful chamber model simulation and needs to be selected with consideration of geometric parameters and fluid conditions of the connected volumes. Several scientific contributions address flow coefficients for certain geometries; a general overview is given by Trutnovsky and Komotori (1981). Besides mass flow measurement (e.g. DIN EN ISO 5167-2:2004), a large field of application of the flow coefficient is the prediction of clearance flow. Several investigations are available for labyrinth seals (e.g. Egli, 1935), where the influence of the moving boundary is assumed to be minor since the movement is crosswise to the fluid flow. Dreißig (1989) performed first experiments with a moving boundary in and against the flow direction and used the results for the simulation of screw machines. Peveling (1987) examined different static geometries in experiments, the results were used as reference for simulation performed by Prins (2004; 2006) and Prins together with Infante-Ferreira (1998; 2003). Bell et. al. (2013) used a one-dimensional approach to predict the flow through clearance passages of scroll compressors and reveal that the real mass flow is likely to be only one percent of the isentropic flow for small clearance gaps and Reynolds numbers.

So far, no detailed investigation of the influence of single parameters on clearance mass flow with one moving boundary has been performed. This paper investigates the two-dimensional fluid flow through front clearances of screw machines, Fig. 1, whereas results can be adopted for other types of rotary displacement machines. The clearance geometry is simplified to the shape of a plane-parallel channel with sharp edges at the inlet and outlet. In order to determine all parameters influencing the flow through the front clearance, the Pi-theorem is used to reduce the number of influencing parameters.

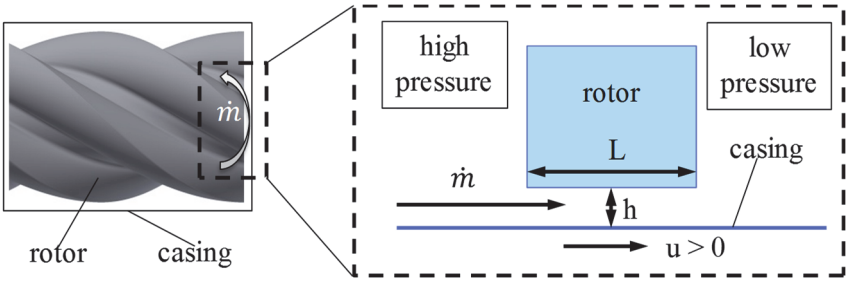

Figure 1. Front clearance geometry of screw machines

2. DETERMINATION OF CHARACTERISTIC NUMBERS

The Pi-theorem, presented by Buckingham (1914), is an approach to reduce the number of independent parameters influencing the system under investigation by performing a dimensional analysis. All physical and geometrical parameters affecting the mass flow rate of the clearance under investigation are summarized in following equation:

$$\dot{m}_{real} = F\left(c_p, c_v, \eta_{hp}, T_{hp}, p_{lp}, p_{hp}, u, L, h, b\right) \tag{4}$$

Fluid parameters (isobaric heat capacity c_p, isochoric heat capacity c_v and dynamic viscosity η_{hp}) are assumed not to vary from the high to the low pressure side. The temperature at the high pressure side can be replaced by the theoretical mass flow (eqs. (1) and (2)) since the equations only depend on considered parameters. The dimensional analysis is performed with independent parameters $\dot{m}_{real}, c_p, p_{hp}$ and h. With some transformations this leads to following characteristic numbers:

$$\Pi_1 = \frac{\dot{m}_{real}}{\dot{m}_{th}} = \alpha,\ \Pi_2 = \frac{c_p}{c_v} = \kappa,\ \Pi_3 = \frac{p_{lp}}{p_{hp}} = \Pi_c,\ \Pi_4 = \frac{2\dot{m}_{real}}{b \cdot \eta_{hp}} = Re,\ \Pi_5 = \frac{h}{L},\ \Pi_6 = \frac{h}{b},\ \Pi_7 = \frac{u}{a_{hp}} = \mathrm{Ma}_u \quad (5)$$

The relationships determined are well known fluid-mechanical parameters. In this study, these are varied systematically for a particular clearance flow in order to show their individual influence on the flow coefficient (Π_1). Fluid flow is investigated by CFD simulation and compared with an analytical approach and experimental data.

3. DETERMINATION OF CLEARANCE MASS FLOW

3.1 CFD simulation

The front clearance mass flow rate is determined by performing CFD-simulation using Ansys CFX© software which uses the finite volume method. Fig. 2 shows an exemplary mesh of the simulated geometry. The high pressure side (length 40 mm, height 30 mm) is defined as an inlet (only allowing incoming mass flow), whereas the low pressure side (length 90 mm, height 30 mm) allows in- and outgoing flows. The length of the clearance remains constant with L = 20 mm, whereas the height h is varied in order to vary Π_5. The width b is constant with one cell of the size of 1 mm and without friction on the front cross sections, so that number Π_6 can be dismissed because the clearance is considered two-dimensional with an infinite width. The boundary is defined as a smooth wall with friction and without heat flux between fluid and solid. Fluids are treated as ideal gases with a constant dynamic viscosity η_{hp} and turbulence is modeled with the Shear Stress Transport (SST) model. The real mass flow rate determined by the CFD simulation is used to calculate the aspired flow coefficient $\alpha_{CFD} = \dot{m}_{CFD} / \dot{m}_{th}$.

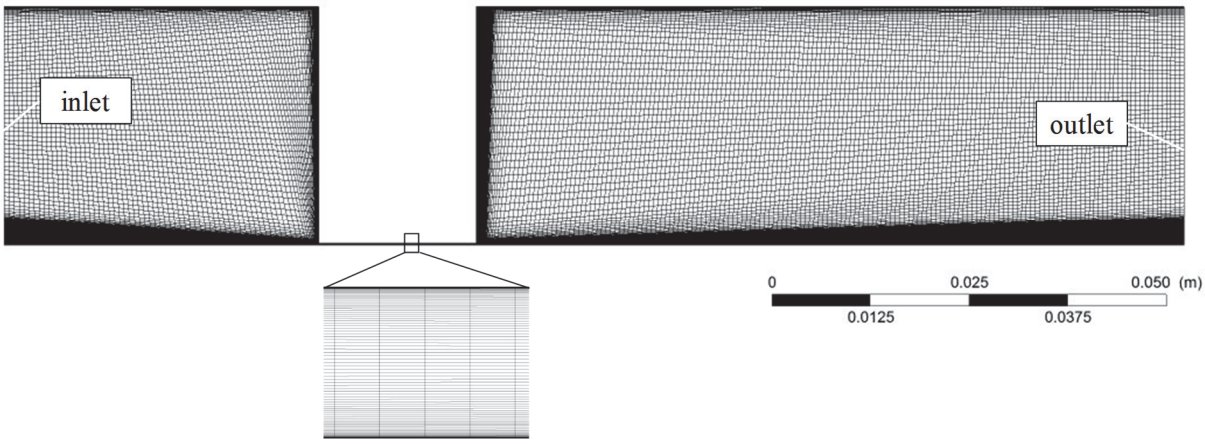

Figure 2. Exemplary front clearance grid

A grid study has been performed together with a Richardson Extrapolation (Ferziger and Peric, 2002) for each geometry under investigation. In the clearance region, there are between 52 and 105 cells in height direction (depending on h / L), whereas small cell heights are used in the wall region in order to capture boundary layer details. The total cell number varies between 130,000 and 216,000. The y+ value is below 2 for all simulation points. The pressure of the outlet and the mass flow rate are used as boundary conditions and are varied systematically in order to achieve a wide variation of Reynolds number (Π_4) and pressure ratio (Π_3). Three different values for the isentropic exponent (1.05, 1.4 and 1.66) are investigated to vary Π_2. A wall velocity can be applied in order to vary the circumferential Mach number (Π_7).

3.2 Analytical solution for static walls

Analytical equations are available for the flow through a rectangular channel for the case of a pure pressure induced, fully developed flow with constant density. Although this is a vague simplification for the compressible clearance flow, it reveals regions of application in which clearance flows can be treated with these simplifying assumptions. The pressure loss due to wall friction in a pipe or channel (length L, hydraulic diameter D_h) can be calculated by (Truckenbrodt, 2008)

$$\Delta p = \lambda \cdot \rho \cdot \frac{L}{D_h} \cdot \frac{c^2}{2} \tag{6}$$

where λ is the friction factor and c the fluid flow speed. With the conservation of mass for steady state flow

$$\mathrm{c} = \frac{\dot{m}_{real}}{\rho \cdot A_c} = \frac{\alpha \cdot \dot{m}_{th}}{\rho \cdot A_c} \tag{7}$$

and with the definition of the hydraulic diameter ($\mathrm{D_h} = 2\mathrm{h}$ for a rectangular channel with infinite width), this leads to the following equation:

$$\Delta p = \lambda \cdot \frac{L}{2 \cdot h} \cdot \frac{\alpha^2 \cdot \dot{m}_{th}^2}{2 \cdot \rho \cdot A_c^2} \tag{8}$$

For laminar flow, the friction coefficient for a rectangular clearance with smooth walls can be calculated by $\lambda = 96 / \mathrm{Re}$ (Truckenbrodt, 2008). Since the Reynolds number is a result of the simulation, the theoretical Reynolds number (calculated with the theoretical mass flow rate, $\mathrm{Re} = \alpha \cdot \mathrm{Re_{th}}$) is used, leading to an analytic equation for the flow coefficient for a pure Poiseuille flow:

$$\alpha_{Po} = \frac{\Delta p}{24} \cdot \frac{h}{L} \cdot \frac{Re_{th} \cdot \rho \cdot A_c^2}{\dot{m}_{th}^2}, \quad Re < 3000 \tag{9}$$

For Reynolds numbers above $\mathrm{Re_{crit}} = 3000$, the Poiseuille flow becomes turbulent (Schlichting and Gersten, 2006) and the friction coefficient can be approximated by the formula from Blasius (Truckenbrodt, 2008), $\lambda = 0.3164/\mathrm{Re}^{0.25}$, leading to:

$$\alpha_{Po} = \left(\frac{\Delta p}{0.3164} \cdot \frac{h}{L} \cdot \frac{4 \cdot Re_{th}^{0.25} \cdot \rho \cdot A_c^2}{\dot{m}_{th}^2} \right)^{4/7}, \quad Re \geq 3000 \tag{10}$$

These equations assume a fluid with constant density, so that an average density between the high and low pressure conditions is used. Since there is no heat transfer assumed between fluid and solid, the change in fluid state inside the clearance takes place with constant total enthalpy. The static temperature in the clearance outlet is reduced by the dynamic temperature, which can be neglected for most simulation points (e.g. 5K for a flow velocity of 100 m/s for air). For this reason, the high pressure side temperature is used to calculate the low pressure density in the last clearance cross section:

$$\rho = \frac{p_{hp} + p_{lp}}{2 \cdot T_{hp} \cdot R_s} \tag{11}$$

Considering this, eqs. (9) and (10) can be transformed so that they only depend on the dimensionless numbers:

$$\alpha_{Po} = \begin{cases} \dfrac{(1-\Pi_c) \cdot (1+\Pi_c)}{48} \cdot \dfrac{h}{L} \cdot Re_{th} \cdot \left(\dfrac{2\kappa}{\kappa - 1} \cdot \left(\Pi_{c^*}^{\frac{2}{\kappa}} - \Pi_{c^*}^{\frac{\kappa+1}{\kappa}} \right) \right)^{-1}, & Re < 3000 \\ \left(\dfrac{(1-\Pi_c) \cdot (1+\Pi_c)}{0.3164} \cdot 2 \cdot \dfrac{h}{L} \cdot Re_{th}^{0.25} \cdot \left(\dfrac{2\kappa}{\kappa - 1} \cdot \left(\Pi_{c^*}^{\frac{2}{\kappa}} - \Pi_{c^*}^{\frac{\kappa+1}{\kappa}} \right) \right)^{-1} \right)^{\frac{4}{7}}, & Re \geq 3000 \end{cases} \tag{12}$$

$$\text{with } \Pi_{c^*} = \Pi_c \text{ for } \Pi_c > \Pi_{crit} \text{ and } \Pi_{c^*} = \Pi_{crit} \text{ for } \Pi_c \leq \Pi_{crit}$$

The equation from Blasius only considers molecular and turbulent friction induced pressure losses; other loss mechanisms (e.g. flow separation at the clearance inlet) which possibly occur are not included. This leads to an overestimation of the mass flow rate for higher Reynolds numbers. Nevertheless, the analytical solution α_{Po} can be adjusted with α_{CFD}, determined by the CFD simulation, to calculate a coefficient α_{inflow}, which includes all losses except friction:

$$\alpha_{inflow} = \frac{\alpha_{CFD}}{\alpha_{Po}} \tag{13}$$

This coefficient will be used for the correction of the estimated mass flow rate with moving boundary.

3.3 Analytical solution for moving walls

The equations presented in section 3.2 are valid for static boundaries, but movement of a boundary causes a Couette flow in the clearance. In screw machines, the fluid is accelerated to the circumferential speed of the machine when entering the working chamber, so that the fluid moves together with the lobes of the rotors. Considering this relative system, it is meaningful to apply the circumferential speed to the casing (as shown in Fig. 1). This additional parameter is considered in the circumferential Mach number (Π_7), which relates the circumferential speed u of the moving boundary to the speed of sound of the high pressure conditions (Dreißig, 1989):

$$\Pi_7 = \frac{u}{a_{hp}} = \frac{u}{\sqrt{\kappa \cdot R_s \cdot T_{hp}}} = Ma_u \tag{14}$$

The circumferential speed in screw machines reaches values up to 100 m/s. Due to the no-slip boundary, the velocity profile of a fully developed Couette flow (laminar or turbulent) can be approximated by means of a triangle with the circumferential speed at one wall and a speed of zero at the opposite wall (Schlichting and Gersten, 2006). For higher Reynolds numbers, inflow losses influence the mass flow rate. It is assumed that the inflow losses reduce the Couette flow in the same way like the Poiseuille flow, so that the pure incompressible Couette mass flow can be estimated by:

$$\dot{m}_{Co} = \frac{u}{2} \cdot \rho \cdot A_c \cdot \alpha_{inflow} \tag{15}$$

For $Re_{Co} = h \cdot u / \nu$ below 1300 the pure Couette flow stays laminar (Schlichting and Gersten, 2006). Since the result of the simulation is a combined Poiseuille-Couette flow, it is assumed that the mass flow rate consists of a Poiseuille part and a Couette part and therefore the Reynolds number is still defined as:

$$Re = \frac{2 \cdot (\dot{m}_{Po} + \dot{m}_{Co})}{\eta \cdot b} = \frac{2 \cdot \dot{m}_{real}}{\eta \cdot b} \tag{16}$$

A critical Reynolds number for this mixed flow is not known. A linear superposition of both flow parts is assumed for the analytical determination of the flow coefficient.

$$\alpha_{Po+Co} = \frac{\dot{m}_{real}}{\dot{m}_{th}} = \frac{\dot{m}_{Po} + \dot{m}_{Co}}{\dot{m}_{th}} = \frac{\alpha_{Po} \cdot \dot{m}_{th} + \frac{u}{2} \cdot \rho \cdot A_c \cdot \alpha_{inflow}}{\dot{m}_{th}} = \alpha_{Po} + \frac{\frac{u}{2} \cdot \rho \cdot A_c}{\dot{m}_{th}} \cdot \alpha_{inflow} \tag{17}$$

Using eq. (11) for the determination of density, the equation can be written in dimensionless form:

$$\alpha_{Po+Co} = \alpha_{Po} + \frac{Ma_u \cdot (1 + \Pi_c)}{4} \cdot \left(\frac{2}{\kappa - 1} \cdot \left(\Pi_{c^*}^{\frac{2}{\kappa}} - \Pi_{c^*}^{\frac{\kappa+1}{\kappa}} \right) \right)^{-1/2} \cdot \alpha_{inflow} \tag{18}$$

with $\Pi_{c^*} = \Pi_c$ for $\Pi_c > \Pi_{crit}$ and $\Pi_{c^*} = \Pi_{crit}$ for $\Pi_c \leq \Pi_{crit}$

3.4 Experiment

A dry air test rig has been assembled in order to experimentally verify the simulation results for static boundaries. The experimental apparatus consists of two large volumes connected by a clearance (as shown in Fig. 2) which can be adjusted in height. Clearance height is measured directly in the clearance at two different positions with capacitive distance sensors. Mass flow rate is measured by means of a Coriolis mass flow meter. The width of the test section is 150 mm; results shown in this paper are obtained for a clearance length of 20 mm. The clearance height has been varied in order to change the height-length ratio.

4. RESULTS FOR STATIC WALLS

4.1 Variation of pressure ratio and height-length-ratio

First results are shown for static boundaries ($Ma_u = 0$). Fig. 3 shows a comparison between CFD simulation and analytical solution for high and low Reynolds numbers. All characteristic numbers remain constant for the progressions except for pressure ratio, which shows a strong impact, especially for low height-length ratios, which result in small mass flow rates dominated by friction. The small flow coefficients for the low Reynolds number indicate that treatment as an isentropic nozzle is not reasonable for small height-length ratios. The assumption of a choked flow, where the pressure ratio is below the critical value (0.528 for air), does not seem valid for Re = 100 since the mass flow rate still increases with lower pressure ratios. Although the pressure ratio is supercritical, the flow speed did not reach the speed of sound of the fluid, so that the mass flow rate still increases with lower pressure ratios.

Agreement between CFD simulation and the laminar analytical solution is excellent and can be explained referring to Fig. 4. The pressure progression for low Reynolds numbers (dashed line) inside the clearance is almost linear and reaches the low pressure conditions in the last clearance cross section. The flow speed when entering the clearance is moderate and a fully developed flow is reached directly after entering the clearance, meaning that inflow losses are negligible ($\alpha_{inflow} \approx 1$).

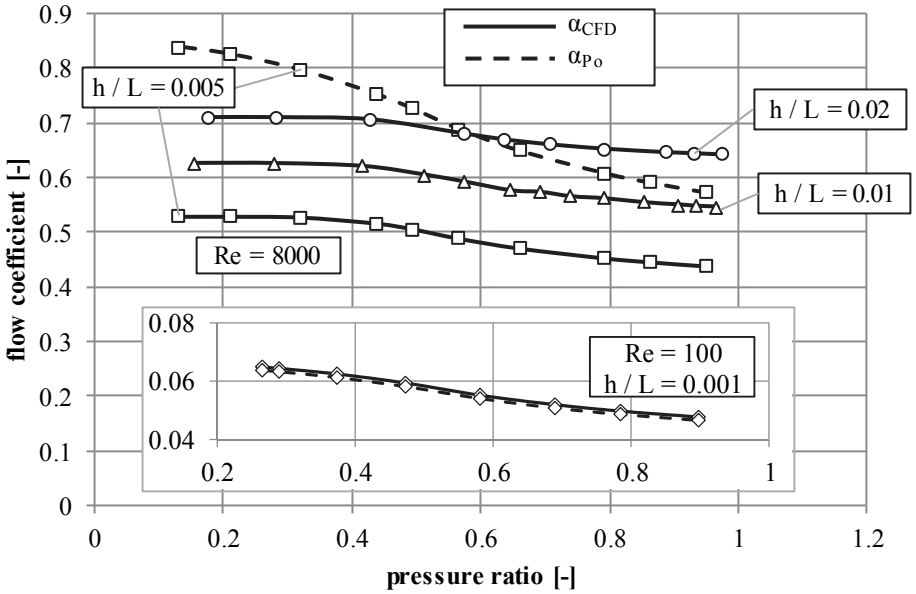

Figure 3. Flow coefficient for dry air ($\kappa = 1.4$) as a function of pressure ratio and height-length ratio for Re = 100 and Re = 8000

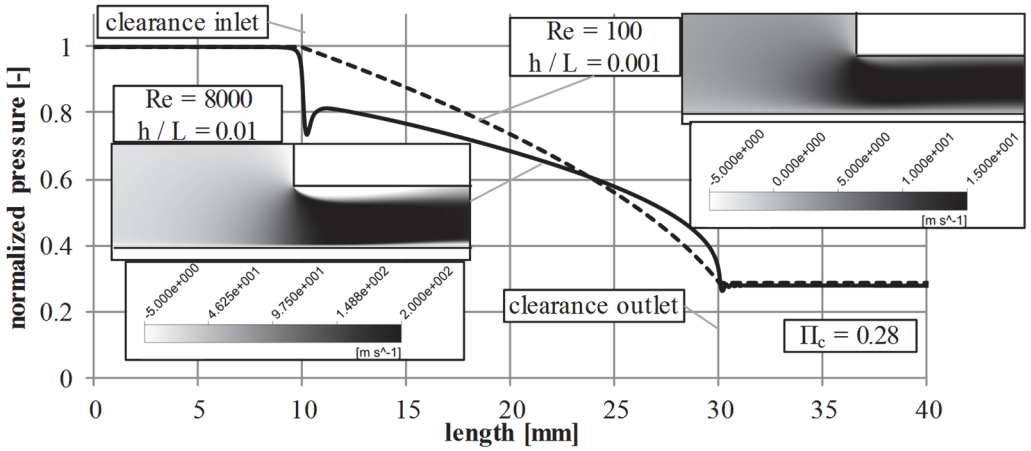

Figure 4. Normalized pressure (p/p_{max}) progression in the front clearance middle height for two different Reynolds numbers with corresponding flow speed (component in clearance length direction) at the inlet

With higher height-length ratios mass flow rate increases, resulting in higher Reynolds numbers. The flow coefficient increases as well with the height-length ratio due to a reduced friction factor. With higher height-length ratio, the pressure ratio, for which a choked mass flow is obtained, increases. This means that the flow reaches the speed of sound at the clearance outlet and a decrease of the low pressure no longer has an influence on the flow inside the clearance. For smaller height-length ratios, the increased friction reduces the flow velocity so that choking of the flow is reached at lower pressure ratios. A comparison between the turbulent analytical solution and CFD simulation for h / L = 0.005 shows that the mass flow rate cannot be predicted for any pressure ratio using the equation from Blasius. As shown in Fig. 4, the higher Reynolds number implies higher mass flow rate and flow speed, leading to a flow separation at the inlet of the clearance; this does not occur for low Reynolds numbers. The flow separation leads to a reduction in available flow cross section, so that the fluid is accelerated and has a vertical velocity component, thereby leading to increased dissipation. Compared to the high pressure conditions, maximum static pressure inside the

clearance is strongly reduced due to this inflow loss. Therefore, the analytical equation leads to higher mass flow values and is not suitable for the prediction of clearance flow for higher Reynolds numbers. Furthermore, the assumption of a linear change in density is not valid anymore.

4.2 Variation of isentropic exponent and Reynolds number

Fig. 5 shows the flow coefficient for a variation of Reynolds number for different isentropic exponents and constant pressure ratio. The flow coefficient increases considerably with Reynolds number. The analytical solution shows good agreement with the CFD simulation for Reynolds numbers below 1000, independent of pressure ratio (not shown) and isentropic exponent, which this comparison shows is obviously not an important parameter. Although the Reynolds number is still below the critical value of 3000, the progressions diverge strongly for Reynolds numbers above 1000, although an investigation of the simulation results revealed that turbulent kinetic energy of the flow is still low. Investigation of the pressure and flow speed progression for Re = 1200 (as in Fig. 4) reveal, that flow separation occurs at the inlet and that the pressure inside the clearance is already reduced.

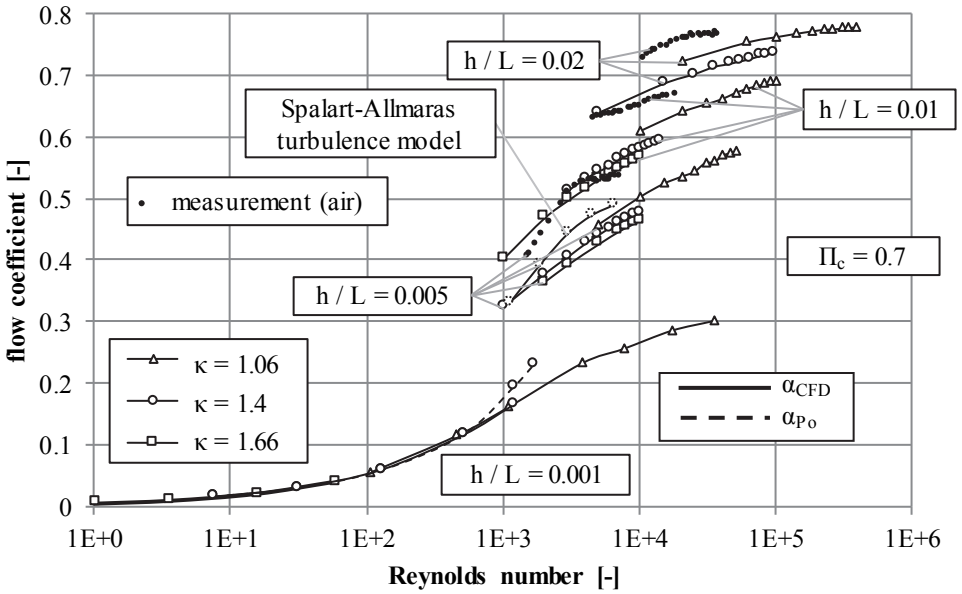

Figure 5. Flow coefficient as a function of Reynolds number, isentropic exponent and height-length ratio for a fixed pressure ratio of $\Pi_c = 0.7$

The height-length ratio has a considerable impact on the flow coefficient. The higher the Reynolds number, the smaller is the boundary layer of the flow so that the averaged flow velocity increases, resulting in a higher mass flow rate. When compared at the same Reynolds number, the flow coefficient decreases with higher isentropic exponents. The calculation of theoretical mass flow (eq. (1)) assumes an isentropic expansion to the low pressure, whereas in the simulation, the change in fluid state is almost isothermal. This indicates that the simulated temperature of fluids with higher isentropic exponent is higher than the isentropic assumption predicts, so that density and mass flow are reduced in the CFD simulation when compared with cases of lower isentropic exponents, since $\kappa = 1$ represents the isothermal case.

The experimental data for air (black dots) shows flow coefficients about 10 percent above the CFD simulation. The experimental Reynolds number is determined using the viscosity at the high pressure conditions determined using the Sutherland equation. The test section clearance surfaces are manufactured by eroding. Measurement of the wall roughness showed values of $R_z \approx 3\mu m$. Additional simulations (not shown) were performed using diabatic walls, wall roughness, and non-constant viscosity; these revealed minor impact. An explanation is the choice of the SST turbulence model selected. Results from use of the Spalart-Allmaras turbulence model for smooth walls are added in the diagram; these show higher flow coefficients than the SST turbulence model, which emphasizes the sensitivity of the turbulent simulation.

An important goal of this work is to have simulation results for the static clearance flow accessible in chamber model simulations. As we have learned, analytical functions (eq. (12)) can be used for Re < 1000. For higher Reynolds numbers, a regression analysis is used to approximate the flow coefficient. Since the Reynolds number depends on

the flow coefficient, the theoretical Reynolds number has been used for the analysis. With consideration of these observations, the flow coefficient can be calculated by

$$\alpha_{CFD,approx} = -1.474 + \sum_{i=1}^{7} \delta_i \cdot \varepsilon_i\,, \quad 0.001 \leq h/L \leq 0.02 \text{ and } 1000 \leq Re = \alpha \cdot Re_{th} \leq 10^5 \tag{19}$$

with parameters δ_i and coefficients ε_i shown in Table 1. 500 Simulation points were used for regression analysis. The formula is consistent with the data; the deviation is less than 5% at 90% of the points.

Table 1: Parameters (δ_i) and coefficients (ε_i) of equation (19) determined by least square method

i	1	2	3	4	5	6	7
δ_i	$\log(Re_{th})^2$	$\log(Re_{th})$	tanhyp(-5·(Π_c-0.5))	κ^2	κ	$(h/L)^{0.25}$	$(h/L)^{0.5}$
ε_i	-0.0327	0.3932	0.03986	0.02534	-0.1484	5.557	-5.974

5. RESULTS FOR MOVING BOUNDARY

The influence of a moving boundary on mass flow rate and flow coefficient is examined in the following for air ($\kappa = 1.4$) for two different height-length-ratios in order to investigate the flow in low and high Reynolds number regions. The results obtained by CFD simulation are compared to analytical functions. Fig. 6 shows results for a low Reynolds number of 655 and a height-length-ratio of 0.001. Eq. (18) is used to determine the analytic flow coefficient. Since the Reynolds number is low, the static flow coefficient α_{Po} is determined using eq. (12) and α_{inflow} equals one. The flow coefficient is strongly influenced by the moving boundary; when the movement remains unconsidered, the error in mass flow can be as much as 100 % for the small height-length ratio under investigation. The influence of the moving boundary is especially notable for higher pressure ratios, where the pressure induced mass flow decreases. As a result, flow coefficient tends to infinity since theoretical mass flow rate and therefore the denominator of the flow coefficient tends to zero. A comparison between CFD simulation and the analytical solution shows acceptable agreement and justifies the usage of the analytical equations to estimate the combined Poiseuille and Couette mass flow for low Reynolds and circumferential Mach numbers. For higher circumferential Mach numbers, the estimated analytical mass flow rates are commonly too high.

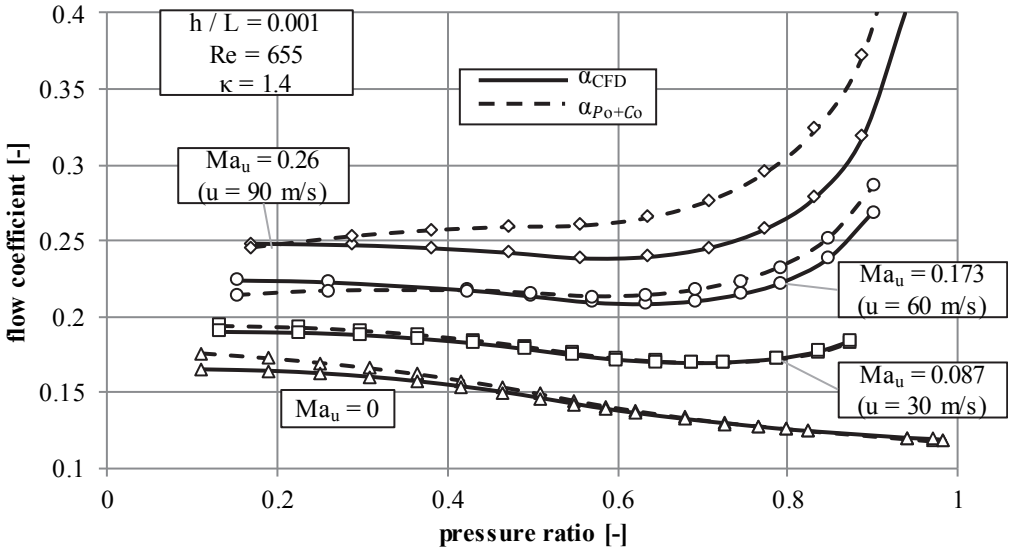

Figure 6. Flow coefficient with moving boundary as a function of pressure ratio and circumferential Mach number for Re = 655, $\kappa = 1.4$ and h / L = 0.001 (T_{hp} = 300 K used for a_{hp})

Results for higher Reynolds numbers are shown in Fig. 7 for an exemplary pressure ratio of 0.25 for a height-length ratio of 0.01. Again, eq. (18) is used to determine the analytic solution, but since Reynolds number is higher, α_{Po} is calculated by means of eq. (19). Together with eq. (12) α_{inflow} can be determined, showing values between 0.45 and 0.7. Results for movements acting against flow direction are added. As for the case of a static boundary, the flow coefficient increases with higher Reynolds numbers. The moving boundary causes a shift of the flow coefficient to

higher mass flow rates for the moving boundary in the flow direction and to lower mass flow rates for movement opposite the flow direction. The agreement between simulated and analytic flow coefficients is better for opposite movement and should be investigated in more detail in future studies. The deviations in general are acceptable and justify the usage of analytical solutions for the Poiseuille-Couette flow in the region of higher Reynolds numbers.

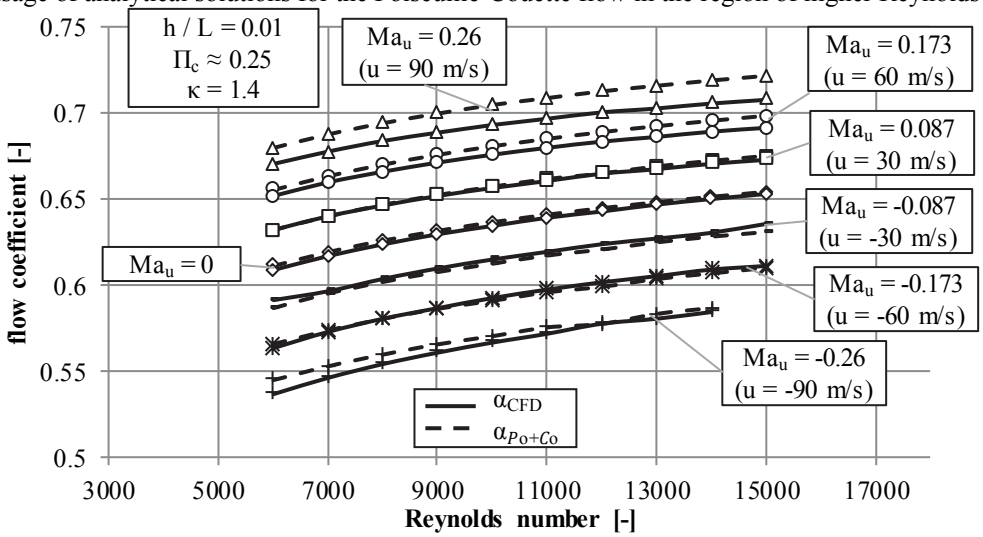

Figure 7. Flow coefficient with moving boundary as a function of Reynolds number and circumferential Mach number for $\Pi_c \approx 0.25$, $\kappa = 1.4$ and $h / L = 0.01$ ($T_{hp} = 300$ K used for a_{hp})

6. CONCLUSIONS

This paper investigates the 2D flow through front clearances of screw machines using a series of characteristic numbers. The flow coefficient is determined using detailed CFD simulation compared to analytical functions and experimental data. Main factors affecting clearance mass flow are height-length ratio, Reynolds and circumferential Mach numbers and pressure ratio. For static clearance flow and Reynolds numbers below 1000, the flow coefficient can be calculated using the analytical equation developed in this study because the flow is mainly influenced by wall friction. For higher Reynolds numbers the flow coefficient increases, but deviation between simulation and analytic solution is greater since the mass flow is strongly influenced by inflow losses. Deviations to experimental data reveal how sensitive clearance mass flow is to the turbulence model used in CFD analysis. A regression analysis has been performed to arrive at an equation for the flow coefficient to make the simulation results accessible, e.g. in chamber model simulation. An investigation of the moving boundary effect revealed a significant impact on mass flow rate. For low Reynolds numbers, the effect of the moving boundary can be estimated analytically by means of a superposition of Couette and Poiseuille mass flow rates with minor errors. For higher Reynolds numbers, the inflow losses need to be taken into account for Couette and Poiseuille flows to represent the flow coefficient in a satisfactory way.

NOMENCLATURE

A	area	(m²)
a	speed of sound	(m/s)
b	width	(m)
c	flow speed	(m/s)
c_p	isobaric heat capacity	(J/kg/K)
c_v	isochoric heat capacity	(J/kg/K)
D_h	hydraulic diameter	(m)
h	height	(m)
L	length	(m)
$\dot{m}$	mass flow	(kg/s)
Ma_u	circumferential Mach number	(-)
p	pressure	(Pa)
Re	Reynolds number	(-)

Subscript

approx	approximated
c	clearance
CFD	CFD simulation
Co	Couette flow
crit	critical value
hp	high pressure
inflow	inflow
lp	low pressure
max	maximal
Po	Poiseuille flow
real	real conditions
th	theoretical condition

R_s	specific gas constant	(J/kg/K)
R_z	average surface roughness	(m)
T	temperature	(K)
u	circumferential speed	(m/s)
α	flow coefficient	(-)
Δ	difference	(-)
η	dynamic viscosity	(Pa·s)
κ	isentropic exponent	(-)
λ	friction factor	(-)
ν	kinematic viscosity	(m^2/s)
Π	characteristic number	(-)
Π	pressure ratio	(-)
ρ	density	(kg/m^3)

REFERENCES

Bell, I. H., Groll, E. A., Braun, J. E., Horton W. T., 2013, A computationally efficient hybrid leakage model for positive displacement compressors and expanders*, Int. J. of Refrigeration* **36**, pp. 1965-1973

Buckingham, E., 1914, On physically similar systems; illustrations of the use of dimensional equations, *Physical Review* **4,** pp. 345-376

DIN EN ISO 5167-2:2004: *Measurement of fluid flow by means of pressure differential devices inserted in circular cross-section conduits running full - Part 2: Orifice plates*

Dreißig, B., 1989, *Ein Beitrag zur Auslegung von trockenlaufenden Schraubenmotoren,* Dissertation, Universität Dortmund.

Egli, A., 1935, Leakage of Steam Through Labyrinth Seals, *Transactions ASME* **57**, no. 3, pp. 115-122

Ferziger, J. H., Peric, M., 2002, *Numerische Strömungsmechanik*, Springer-Verlag, Berlin Heidelberg New York

Kauder, K., Janicki, M., Rohe, A., Kliem, B., Temming, J., 2002, Thermodynamic Simulation of Rotary Displacement Machines, *VDI-Berichte 1715*, VDI Verlag, Düsseldorf, pp. 1-16.

Peveling, F.J., 1987, *Ein Beitrag zur Optimierung adiabater Schraubenmaschinen in Simulationsrechnungen,* Dissertation, Universität Dortmund

Prins, J., Infante Ferreira, C. A., 1998, Quasi One-Dimensional Steady-State Models for Gas Leakage Part II: Improvement of the Viscous modeling, *International Compressor Engineering Conference at Purdue, paper 1302*

Prins, J., 2004, Boundary Layer Leakage Model, *International Compressor Engineering Conference at Purdue, paper 1696*

Prins, J., 2006, On the Structure of Compressor Gas Leakage Flows, *International Compressor Engineering Conference at Purdue, paper 1728*

Prins, J., Infante Ferreira, C. A., 2003, Selected basic theory of gas leakage, *Int. Conf. on Compr. And their Systems,* IMechE Conference Transaction, London, pp. 521-530.

Rane, S., Kovacevic, A., Stosic, N., Kethidi, 2014, Deforming grid generation and CFD analysis of variable geometry screw compressors, *Computers & Fluids*, vol. 99, pp. 124-141

Schlichting, H., Gersten, K., 2006, *Grenzschichttheorie*, Springer-Verlag, Berlin Heidelberg

Saint Venant A. J. C., Wantzel L., 1839, *J. de l'Ecole Roy. Poly.* **16**, (series 1) 85

Truckenbrodt, E., 2008, *Fluidmechanik*, Springer-Verlag, Berlin Heidelberg

Trutnovsky, K., Komotori, K., 1981, *Berührungsfreie Dichtungen*, VDI-Verlag, Düsseldorf

ACKNOWLEDGEMENT

The work leading to these results has received funding from the European Community's Horizon 2020 Programme (2014-2020) under grant agreement no 678727. The opinions expressed in the document are of the authors only and no way reflect the European Commission's opinions. The European Union is not liable for any use that may be made of the information.